# Fabrication of flexible energy harvesting device based on BCZT Nano-ceramics

A dissertation submitted in fulfilment of the requirements for the degree

Of

**MASTER OF SCIENCE**

*In*

**PHYSICS**

*Submitted by*

Qaiser Yousuf

Roll No. 301704024

*Under the Guidance of*
Dr Jayant Kolte,
Asst. Professor, SPMS


**2019**

**School Of Physics and Material Science**
**Thapar Institute of Engineering & Technology, Patiala**
***(Declared as Deemed-to-be-University u/s 3 of the UGC Act., 1956)***
**Post Bag No. 32, Patiala – 147004 Punjab (India)**

# CERTIFICATE

Certified that the dissertation entitled, **"Fabrication of flexible energy harvesting device based on BCZT Nanoceramics"**, which is being submitted by **Qaiser Yousuf (301704024)** in fulfilment of the requirements for the award of the **M.Sc Physics**, to Thapar Institute of Engineering & Technology (Deemed to be University), is a bona-fide record of the candidate's own work carried out by him under my supervision and guidance. The matter contained in this dissertation has not been submitted, neither in part or in full to any other university or institute for award of any degree.

Place: Patiala, Punjab

Date: 29/8/19

**(Dr. Jayant Kolte)**

**supervisor**

# ACKNOWLEDGMENT

First of all, I would like to thank to the Almighty Allah, who is the creator of this universe and it is his mercy and blessing to me that this work become possible.

I would like to express my sincere gratitude to my supervisor **Dr. Jayant Kolte** for his unlimited guidance, insight and suggestions throughout the research. I thank him from the bottom of my heart for introducing me to the area of electro ceramics. I thank him for his great patience, constructive criticism and myriad useful suggestions apart from invaluable guidance to me.

I am grateful to **Dr O.P. Panday**, Head of School of Physics and Material science (SPMS) for his encouragement and help to carry out the thesis work.

I am also indebted to my senior research colleague **Mr Savidh Khan** for his unconditional support and constant motivation whenever needed.

I am very grateful to my dear friend **Mr Raman Kumar** who has given me his friendship, put up with my odd hours, and provided me with lifts and practical help.

Last but not the least; I would like to thank my dear parents, my elder brother and my beloved Sister's for their support, without their support it was not possible to come so far.

**QAISER YOUSUF**

**(301704024)**

# DECLARATION

I hereby certify that the work which is presented in dissertation entitled, "**Fabrication of flexible energy harvesting device based on BCZT Nanoceramics**", in partial fulfilment of the requirement for the award of the degree of Masters In Physics, School of Physics and Material Science, Department of Thapar Institute of Engineering & Technology (Deemed to be University) is as authentic record of my own work carried under the supervision of **Dr.Jayant Kolte.** It refers others researcher's work which are duly listed in the reference section. The matter contained in this dissertation has not been submitted, neither in part or in full to any other degree to any other university or institute except as reported in text and references.

Place: Patiala
Date: 29/08/2019

**(Qaiser Yousuf)**
**Roll No.: 301704024**

It is certified that the above statement made by the student is correct to the best of my knowledge and belief.

Date: 29/8/19

**(Dr. Jayant Kolte)**
**Assistant Professor**
School of Physics and Material Science,
Thapar Institute of Engineering & Technology, Patiala

# ABSTRACT

Barium calcium zirconate titanate ($Ba_{0.85}Ca_{0.15}Ti_{0.9}Zr_{0.1}O_3$, BCZT) ceramic have been successfully synthesised by sol-gel method. Thermogravimetry analyser is used for the confirmation of Calcination temperature of the synthesised BCZT powder i.e. 900℃. The powder calcined at 900℃, to obtain the single phase perovskite structure. The flexible nanocomposite films of BCZT/ Polyvinylidene fluoride (PVDF) has been fabricated by solution casting method. The microstructure and the morphology have been studied by SEM and optical microscope. The particle are homogenously dispersed in the PVDF matrix as confirmed by SEM. Optical microscopy images revealed that the PVDF film with 50 wt% is less porous as compared to others. Formation of the $\beta$-phase is confirmed by the X-ray diffraction and Fourier transform infrared (FTIR) spectroscopy. The dielectric constant increases with increase in wt% of BCZT in PVDF. The highest dielectric constant is 91.35 and tanδ is 0.05 at 1 KHz.

# TABLE OF CONTENTS

# List of figures

# CHAPTER 1
## Introduction

## 1.1 Energy harvesting

Energy is defined as the capacity of doing work. The process of acquiring energy from the surrounding environment has been a continuous human effort throughout history. Common sources of energy harvesting are mechanical energy from source due to mechanical stress, strain and vibrations, thermal energy due to the kinetic energy of the atoms or molecules , light energy captured from the sunlight with the help of photo sensors, photodiodes etc.

Energy harvesting from the environment has received much attention to address the major problem of the energy crisis. This problem has been addressed by the various approaches like thermal, solar, pyroelectric and piezoelectric energy harvesting techniques [1-2]. The well known approach for the energy harvesting is the piezoelectric nanogenerators which can generate the energy from different sources like wind, hydro, motions. The generated power has the wide range of application in the electronic devices such as LEDs, mobile, sensors etc. Simultaneously the generated energy can be stored in the capacitors or batteries which are assembled with the nanogenerators. Different materials have been investigated for this application such as Zinc Oxide (ZnO), Zinc Stannate ($ZnSnO_3$), Lead Zirconate Titanate (PZT), Barium titanate (BT) [3-8] etc. in different forms like nanocomposite, nanowire and nanofibres. Out of these, composites are more common because for the enhancement of the output voltage and different designs of the device can be easily adapted. The lead based (PZT) composite are known to have the exceptional piezoelectric properties and they can produce the maximum voltage [9]. As there is lead present in these composite which is hazardous to the mankind and environment. So, the replacement of the material is necessary. Extensive research has been done to find an alternative for the lead based composites. Lead free piezoelectric materials such as KNN, BT have relatively high piezoelectric properties [10]. The lead -free piezoelectric ceramics can be categorized into three type's tungsten bronze, bismuth layer, perovskite structures. The lead-free piezoelectric ceramics which are most widely studied can be categorized into three types according to their structures: tungsten bronze, bismuth layer, and perovskite structures. The most studied piezoelectric materials which are having the perovskite structure are ($K_{0.5}Na_{0.5}$)

$NbO_3$ (KNN), $(Bi_{0.5}Na_{0.5})$ $TiO_3$ (BNT), and $BaTiO_3$ [11]. The KNN has high Curie temperature ($T_c$ = 420℃), large electromechanical coupling factors and good ferroelectric properties (Pr = 33 μC/cm$^2$) due to the low melting point of $KNbO_3$, KNN can't be sintered under the atmospheric condition. NBT is also considered as the promising candidate for lead-free Piezoelectrics but due to coercive field and high conductivity polling process becomes hard [12]. BT system has highest piezoelectric coefficient (d33 ~ 190 PC/N) and high electromechnical coupling factor among all the lead-free systems but due to low Curie temperature (Tc) and number of polymorphic phase transitions restricts its usage in temperature range [13-14]. From past few years, a new material Barium Calcium Zirconate Titanate (BCZT) is found one of the promising alternatives for the lead free Piezoelectrics (PZT) which show high piezoelectric coefficient ($d_{33}$ ~ 620 PC/N). Coexistence of the Rhombohedral and the tetragonal phases at the Morphotropic phase boundary (MPB) has been reported [15-16]. The fabrication of the film is done by using the inorganic materials and the piezoelectric polymers like PVDF (Polyvinylidene fluoride) and its co-polymers. The polymers has dual role. They hold the nanoparticles and being a piezoelectric material it also contributes to the generation of the electric energy [17]. PVDF polymer exists in the four crystalline phases viz α, β, γ and δ phases. Out of these four phases β and γ are electro active phases and have high piezoelectric properties. Out of these α-phase is non-polar due to molecular dipoles are anti-parallel to each other and exhibit zero net dipole moment. Out of all the four phases of PVDF, β-phase is found to have dipole moment of 2.10 D which is highest among all the phases. The piezoelectric ceramics has to be embedded into the polymer for flexible devices. Thus with the combination of the PVDF/BCZT composites facilitates the application of the nanogenerators [18-19]. The main aspect for the piezoelectric energy harvesters are piezoelectric charge constant ($d_{33}$) and piezoelectric voltage constant ($g_{33}$), their magnitude ($d_{33}.g_{33.}$) will define the efficiency of the harvester. In this case the composite consists of the PVDF/BCZT in which BCZT is known for the high piezoelectric charge constant ($d_{33}$ ~ 620 pC/N ) and PVDF is known for possessing the high piezoelectric voltage constant ($g_{33}$ ~ 0.14–0.33Vm/N) among all the polymers [20]. So, the composite PVDF/BCZT will serve as an efficient energy harvester. This electric energy generated can power the small devices. In this work we have focused on the ferroelectric polymers such as Polyvinylidene fluoride (PVDF) and its copolymers. These have very high potential for energy harvesting because of flexible, light weight, easy and cheap and easy to fabricate and these are also environmental friendly. Due to the high efficiency and low cost piezoelectric

polymer NGs, these could lead to the energy solutions to various electronic and wireless devices.

## 1.2 Piezoelectrics

The ability of the certain crystalline materials to develop the electric charge on applying the mechanical stress or vice-versa is called the piezoelectricity. Piezoelectricity means the electricity generated due to the pressure. Piezoelectricity is derived from a Greek word piezo which means to press or squeeze. The internal generation of the electric charge due to the applied mechanical force is called the direct piezoelectric effect while as the mechanical strain due to applied electric field is known as converse piezoelectric effect. The crystals which have the ability to produce electric field when the mechanical force is applied on them are called the piezoelectric crystals. The origin of the piezoelectricity in the crystals is due to the displacement of the ionic charge which leads to the polarisation and the electric field. The crystals which don't have the centre of the symmetry when exposed to the mechanical stress , the positive and the negative ions gets deformed and the electric dipoles are induced which in turn produce electric field. The induced polarisation direction depends only on the direction of the applied stress. Due to the unique properties of the piezoelectric materials they have been utilized in the fabrication of the various types of the electronic devices like piezoelectric sensors, piezoelectric transducers etc. Devices which are based on the piezoelectric have wide range of application in the consumer products to the scientific equipments [1].

## 1.3 Piezoelectric effect

The substance which produces an electric charge upon the application of the mechanical stress is called piezoelectric crystal and vice-a-versa. When the stress is applied there is the generation of the electric charge in the material which is called the direct piezoelectric effect, it was discovered by Jacques and Pierre Curie in 1880. Fig 1.1 shows a simple model which explains the direct piezoelectric effect. When the external stress is not applied, the positive and the negative centres coincides, there is no separation of the charges so the material represents the electro neutrality. When stress is applied, there occurs the separation the positive and the negative charge which results in the little dipole moment. The positive and the negative charges get separated and get accumulated on the two parallel surfaces of the material which generates the electric field.

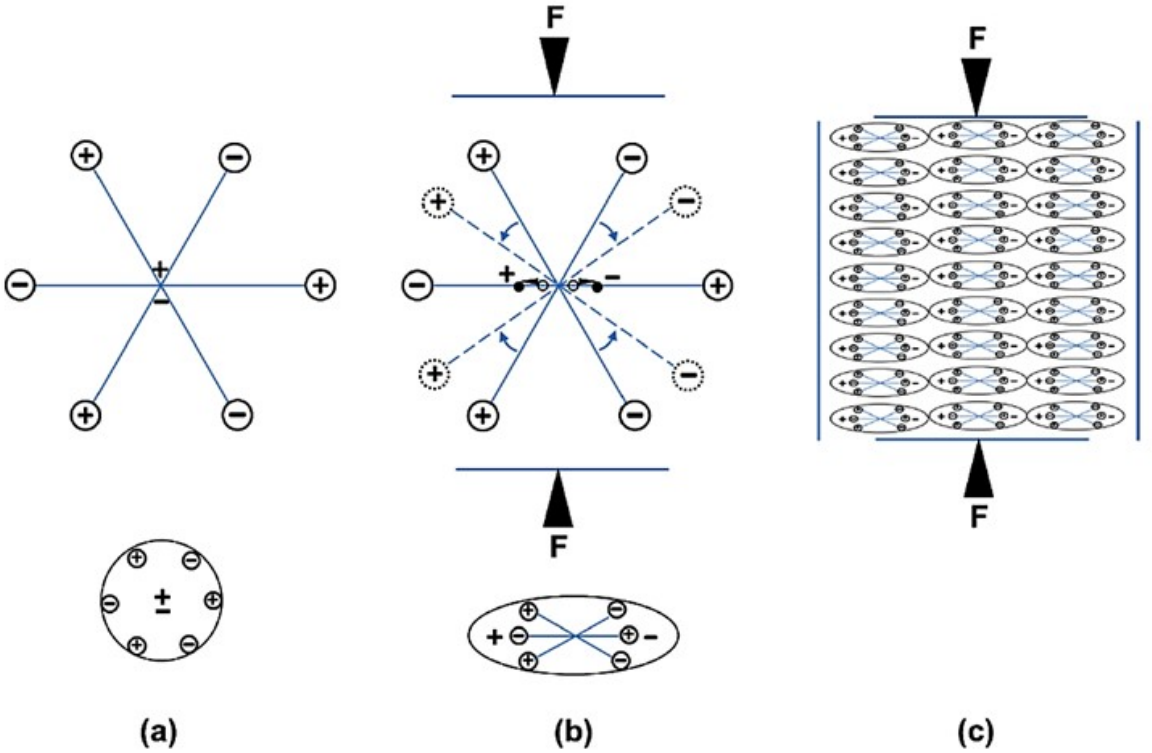


**Fig 1.1. (a) Unperturbed molecule; (b) Molecule subjected to an external stress; (c) Electric field generated on the material surfaces** [Ref.1]

The production of the stress or strain when an electric field is applied is called the converse piezoelectric effect; it was discovered in 1881 and was confirmed by curie brothers. When there is change in the stress from tensile to the compressive, there is reverse in the sign of electric charge for direct piezoelectric effect and when there is change in the direction of the electric field for converse piezoelectric field, then strain will reverse its sign. If the coupling occurs between the shear mechanical stress and stain the shear piezoelectric effect exists [1]. These phenomenon direct, converse, and shear piezoelectric effects are demonstrated in Fig 1.2

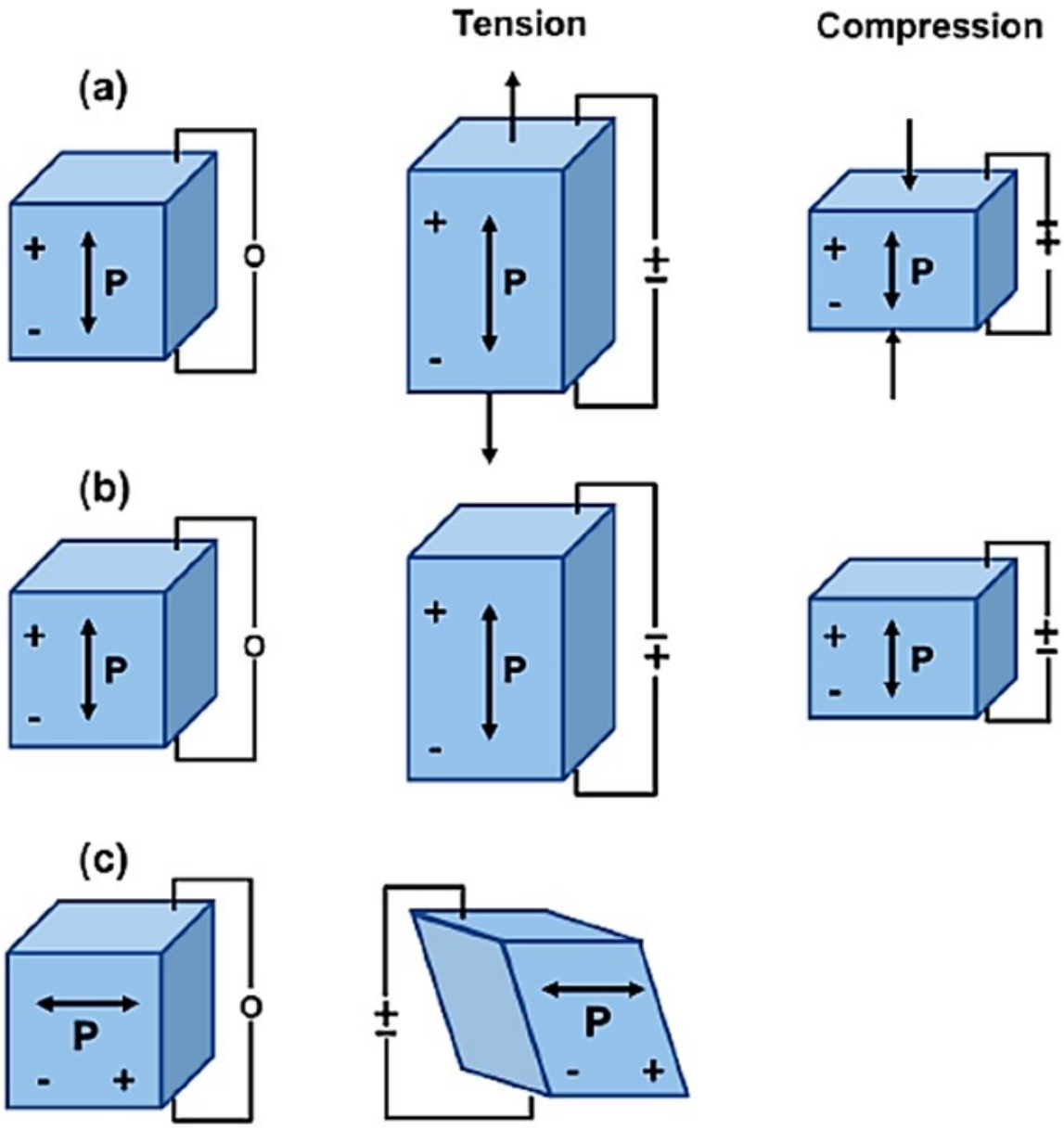


**Fig 1.2, (a) converse (b), and shear (c) piezoelectric effects**.[Ref 1]

## 1.4 Piezoelectric and subgroup

On the bases of the symmetry the crystals are classified in to 32 point groups , these 32 point groups are then sub-divided in to 7 basic crystal systems which are; triclinic, monoclinic, orthorhombic, tetragonal, rhombohedral (trigonal), hexagonal and cubic. These point groups can be divided on the basis of centre of symmetry and without centre of symmetry, 21 point groups are non-centrosymmetric and out of these 20 exhibits the piezoelectricity and 10 crystal classes are designated as pyroelectric. The pyroelectric group of materials posses the

characteristic to be permanently polarized in a given range of temperature. Whereas in piezoelectric classes the polarization is produced under the applied Stress.

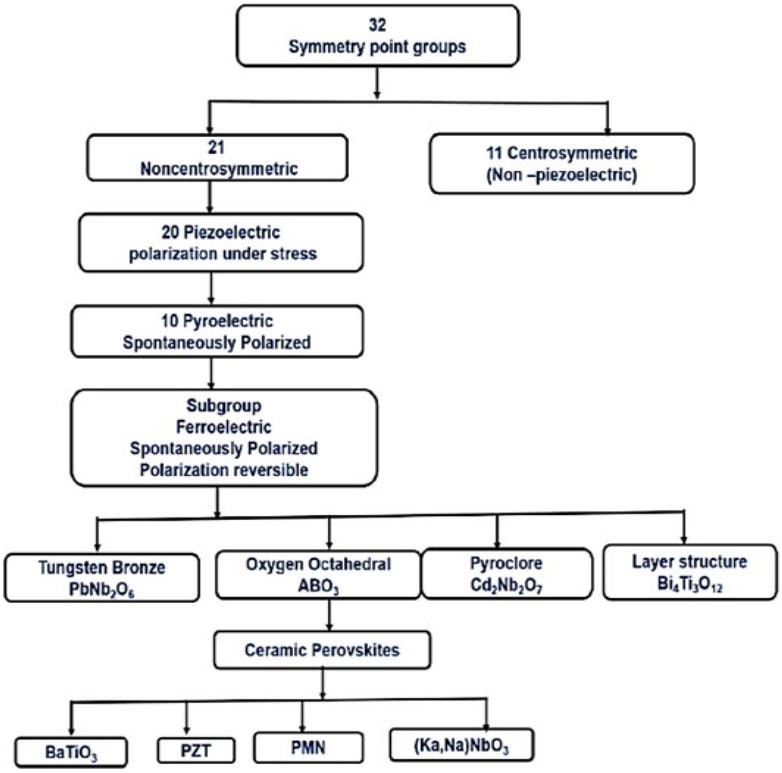


**Fig 1.3 piezoelectric subgroups**

## 1.5 Lead-free piezoelectric ceramics

On the bases of structure lead -free piezoelectric ceramics can be categorized into three type's tungsten bronze, bismuth layer, and perovskite structures. The lead-free piezoelectric ceramics which are most widely studied can be categorized into three types according to their structures: tungsten bronze, bismuth layer, and perovskite structures. The most studied piezoelectric materials which are having the perovskite structure are $(K_{0.5}Na_{0.5})$ $NbO_3$ (KNN),

$(Bi_{0.5}Na_{0.5})$ $TiO_3$ (BNT) and $BaTiO_3$. Fig 1.4 represents these three types of

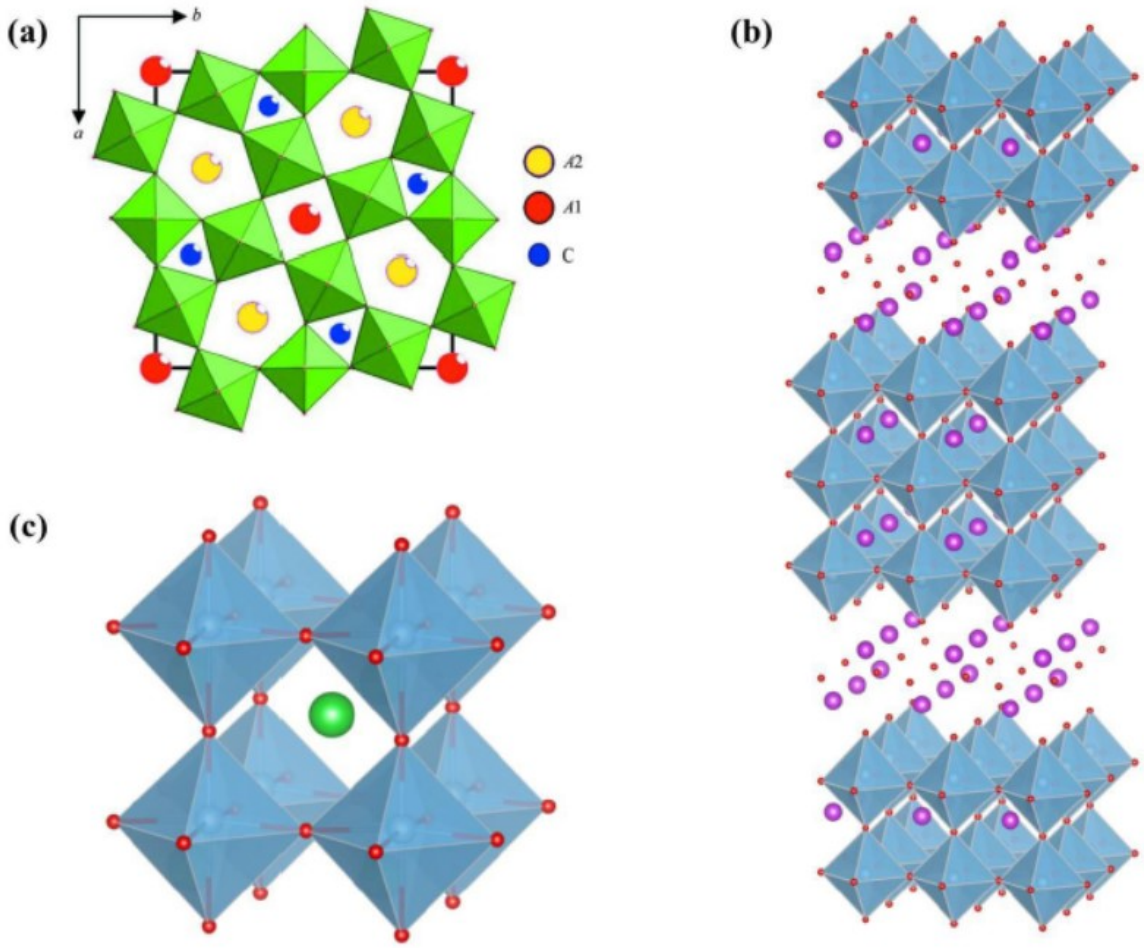


**Fig. 1.4, (a) Tungsten bronze structure; (b) Bismuth layered structure; (c) Perovskite structure.**[Ref 1]

Out of these tungsten bronze and bismuth layered structure has high Curie temperature (*T*c), high mechanical quality factor ($Q_m$), large dielectric breakdown strength, and good aging characteristics which makes them suitable lead-free candidate materials for wide applications. They possess poor piezoelectric properties and dielectric permittivity piezoelectric which is possible due to the structural anisotropy. While as lead-free piezoelectric materials has good piezoelectric properties as there is spontaneous rotation of polarization along 3D-orientations i.e. x, y, z directions that is why for the piezoelectric application perovskite structures are focused for the lead free substitution [1].

## 1.6 BCZT Ceramics

The lead-free perovskite structures can be classified in to three main types: (1) $K_{0.5}Na_{0.5}NbO_3$ (KNN), (2) $Na_{0.5}Bi_{0.5}TiO_3$ (NBT), and (3) $BaTiO_3$ (BT). The KNN has high Curie temperature ($T_c$ = 420 ℃), large electromechanical coupling factors and good ferroelectric properties (Pr =33 μC/cm$^2$) due to the low melting point of $KNbO_3$, KNN can't be well-sintered under the atmospheric condition. NBT is also considered as the promising candidate for lead-free Piezoelectrics but due to coercive field and high conductivity polling process becomes hard in it. BT system has highest piezoelectric coefficient (d33 ~ 190 pC/N) and high electromechnical coupling factor among all the lead-free systems but due to low Curie temperature (Tc) and number of polymorphic phase transitions restricts its usage in temperature range. BCZT which belongs to the $BaTiO_3$ ceramics system which is perovskite structure, $Ba^{2+}$ and $Ca^{2+}$ ions occupies the A-sites while as the B-sites are occupied by $Zr^{4+}$ and $Ti^{4+}$.

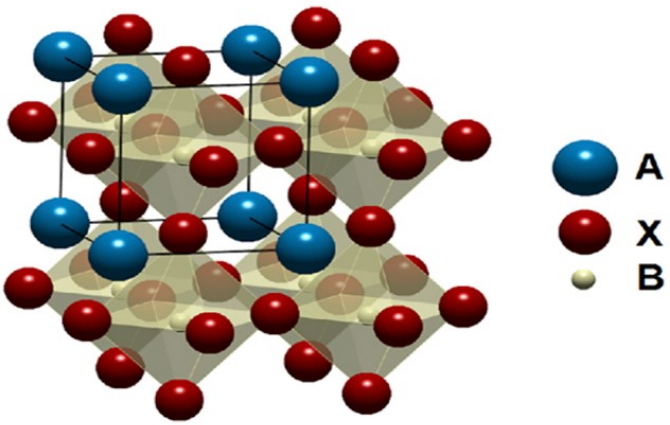


**Fig 1.5 Diagram of prototype perovskite structure: A = B $^{2+}$, Ca$^{2+}$ B = Zr$^{4+}$, Ti$^{4+}$; X = O$^{2-}$** [Ref 21]

As there is no volatile element present in the BCZT composition, the stiochiometric ratio is well maintained after the high calcining / sintering temperatures and the environmental friendly characteristics and the piezoelectric properties makes it the prospective candidate for the lead-free Piezoelectrics [21].

## Advantages of BCZT

- BCZT has the electromechanical properties comparable to PZT
- High piezoelectric coefficient($d_{33}$) (~620 pC/N), is obtained in BCZT ceramics
- BCZT does not have any volatile elements
- BCZT ceramics exhibit dielectric constant values as high as ~18 000

## 1.7 Polyvinylidene fluoride (PVDF)

PVDF is the vinylidene fluoride polymer and contain 59.4% by weight of fluorine and 3% by weight of hydrogen atoms and also the crystallinity of about 50−70%. The range of the glass and melting temperatures is −40 to −30 °C. For PVDF the Curie temperature lie in the range of 195−197 °C .The semi crystalline polymer PVDF exists in five phases which are α, β, γ , δ and ε. Out of these α-phase is non-polar due to molecular dipoles are anti-parallel to each other and exhibit zero net dipole moment. Remaining β, γ, δ and ε are polar as there molecular dipoles are parallel to each other, hence the net dipole moment is not zero.

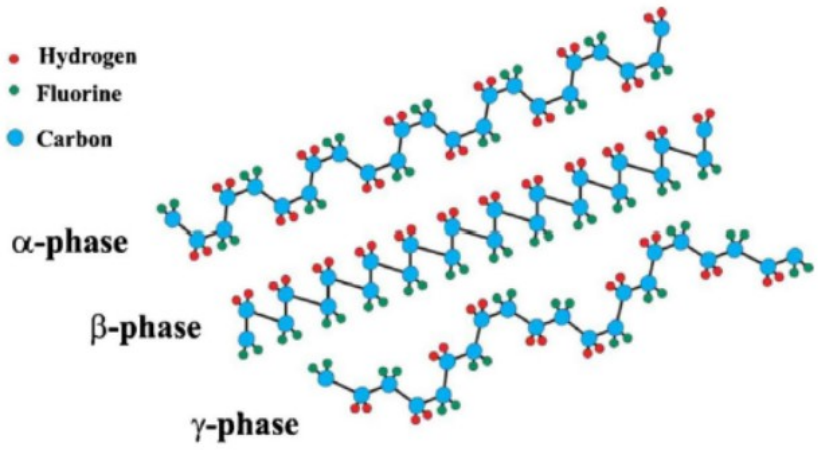


**Fig 1.6 Representation of different phases of PVDF**.[Ref 20]

Out of all the five phases of PVDF, β-phase is found to have dipole moment of 2.10 D which is highest among all the phases, the dipole moments of α, γ, and δ-phases are 1.02 and 1.20D which is in parallel and perpendicular to the direction of chain length. Also it is found that the dielectric constant of PVDF lies in between 6−12 [20]

**Physical properties of PVDF**

- Specific gravity : 1.75 -1.80;
- Melting point : 154-184$^0$ C;
- Water absorption : 0.04-0.06%;
- Tensile strength at break : 36-56 M pa;
- Elongation at break : 25-500%,
- Low temperature embrittlement : -62 to 64$^0$ C.

## Electrical Properties of PVDF

- Volume resistivity : 2x10$^{14}$ ohm-cm;
- Dielectric constant at 60 Hz : 8.40 pm/V
- Piezoelectric stress constant : 0.23V/ (m. pa)
- Voltage coefficient $g_{33}$ : 0.14–0.33Vm/N

# Chapter 2
## Literature

## 2.1 Literature review

Piezoelectric [$x$BZT–(1−$x$)BCT] (0.48 ≤ $x$ ≤0.52), has been synthesized via sol–gel method. Calcination of synthesised powder performed at 700$^{o}$c, which is very much lower compared to solid-state reaction. Composition of, 0.5BZT–0.5BCT, att the Morphotropic phase boundary have high coercive field ($Ec$) of 0.14 kV/mm and remnant polarization ($Pr$) of 12.2 μC/cm$^2$. $d_{33}$ nearly 637 PC/N resulted due to optimized poling conditions, has large coupling coefficient $kp$ nearly 59.6%, a high piezoelectric voltage constant $g_{33}$~29 mV m/N for BCZT[23].

BCZT has been synthesised by the sol-gel method. The ceramics of BCZT was calcined at 1000$^{0}$c and was sintered at the temperature of 1420℃ , it was well dense and grain size. The results obtained for the dielectric and ferroelectric property of BCZT synthesised using sol-gel method were compared with the SSR method. The optimum electrical results with the values of $d_{33}$ = 504 PC/N, KP= 0.56, $e_m$ = 16, 480, Ps = 17.76 l μC/cm $^2$, Pr = 11.64 l C/cm $^2$, W = 0.52 J/cm $^3$. These materials find the real applications in the capacitors. All the results obtained shows that these materials have the great prospective in the Piezoelectrics [24].

BCZT preparation by the wet chemical method was investigated and the powder was used to find the relationship between the piezoelectric properties and the microstructure of sintered BCZT ceramics. It was observed that the sol-gel method is successful method for the preparation of BCZT nanoparticles with tetragonal perovskite phase. There was the decrease in the grain size from 0.8-0.9μm when the cold isostatic pressing was used. By sintering the BCZT ceramics at wide range of sintering schedules, wide range of grain size 0.8-60.51μm where obtained. The ceramics which was prepared by the sol-gel method and sintered at 1425$^{0}$c has highest $d_{33}$ = 410.8 ± 13.2 pC/N with the relative density of 89.6% theoretical density and 361μm grain size [25].

Yang et-al investigated in detail the effect of the structural properties of BZT-BCT lead-free solid piezoelectric solutions and found several important factors related to BZT-BCT. By using the Varity of sintering temperatures and procedures ceramics of BZT-BCT were fabricated. The obtained samples where well dense and their average grain size was inhibited by varying the first particle size and rate of cooling during the sintering temperature. On the other hand the structural parameter c/a ratio in tetragonal phase is not depending on sintering. The constructed

phase diagram was based on the phase transition as identified by the dielectric property measurements. By the variation of the grain size and tetragonal phase c/a ratio, the piezoelectric properties were modified. It was observed that $d_{33}$ values increase with increase of c/a ratio [26].

By using the Tape casting technique followed by the hot press, the PVP modified BCT-BZT nanocomposite were fabricated. The devices performance which was made with the different concentration of BCZT powder in the PVDF matrix has been studied by harvesting energy with human hand palm force. The output dc voltage of 6V and the short circuit current of 94μA were obtained. It was found that this device is able to glow fifty five LEDs. Thus this work shows that these composite has great future in self powered sensors [1].

The changes in the β-phase content of the PVDF thick films is achieved when the PVDF solution is baked at the different temperature and spin coated at different spin speeds. Up to the baking temperature of $60^0$c β-phase is dominant after this temperature the β-phase decreases and the α-phase start increasing and is dominant up to 90 $^0$c. By increasing the temperature the porosity decreases. [27].

Wang-et-al has studied the effect of dopamine on the BCZT/PVDF composite films. Solution casting method was used for the preparation of the flexible BCZT/PVDF composite films which are having the high dielectric constant and low dielectric loss. To know whether the dopamine is uniformly coated on the surface of the BCZT particles. By increasing the concentration of the BCZT the dielectric constant increases and the loss tangent remains constant in the frequency range of $10^3$ to $10^5$ Hz [28].

Sadhu et-al studied the dielectric properties and energy storage density of BCZT/PVDF-HFP composite films. With the help of the sol-gel method they synthesised the polymer nanocomposite with the different volume concentration of the BCZT. [29].

Crossley et al. studied the energy harvesting of flexible nanogenerators which have the application in the wireless sensors, portable and wearable devices. The energy harvester devices based on the Piezoelectrics and are of nanoscale which is also known as nanogenerators (NGs), these nanogenerators can convert the vibrations into electric energy. This electric energy generated can power the small devices. In this work they focused on the ferroelectric polymers like Polyvinylidene fluoride (PVDF). These have very high potential for energy harvesting because of flexible, lightweight, easy and cheap and easy to fabricate and these are also environmental friendly. Due to the high efficiency and low cost piezoelectric polymer NGs, these could lead to the energy solutions to various electronic and wireless [30]

Kou et-al worked on the flexible piezoelectric nanogenerators, which were fabricated by mixing the nanoparticles of the BCZT ($0.5Ba(Zr_{0.2}Ti_{0.8})O_3$-$0.5(Ba_{0.7}Ca_{0.3})TiO3$) PDMS polymer

matrix. The fabricated device shows the excellent performance with 0.6 V of open circuit voltage and the short circuit current of 7.5na. [31].

By using the solution casting method, $Ba_{0.95}Ca_{0.05}Zr_{0.15}Ti_{0.85}O_3$/PVDF composite films which have high dielectric constant and low dielectric loss were fabricated with BCZT powders as fillers. With the increase in the concentration of the BCZT, the dielectric constant increases while as the loss tangent remains constant in the frequency range of $10^3$ to $10^5$ Hz [32].

M.K Gupta-et-al studied the performance of the lead free $Na_{0.47}K_{0.47}Li_{0.06}NbO_3$ (NKLN) based generators for the energy harvesting. They fabricated the device using the NKLN: PDMS composite structure for power generation. The result for the output voltage was 48 V and the current 0.43 µA/ $cm^2$ [33].Some of the key parameters of lead free piezoelectric ceramics are depicted in table 2.1

## Table 2.1 summary of some important parameters

| Material | $d_{33}$ pC/N | $\varepsilon_r$ | $P_r$ (µC/$cm^2$) | Current(nA) | Voltage(v) | Power(µW) | Energy storage density(J/ $cm^3$) | Year | Reference |
|---|---|---|---|---|---|---|---|---|---|
| BCZT and PVDF | ... | ... | ... | ... | ... | ... | ... | 2014 | **[28]** |
| BCZT/PVDF-HFP | ... | ... | ... | ... | ... | ... | 8.5 | 2018 | **[29]** |
| NKLN/PDMS | 460 | ... | 13.66 | 0.43 | 48 | ... | ... | 2016 | **[33]** |
| PVDF- Zno | -1.17 | ... | ... | 0.5 | -1.81 | 0.21 | ... | 2018 | **[34]** |
| P(VDF-HFP) AND $ZN^{2+}$ | ... | ... | ... | ... | 6 | 2.4 | ... | 2017 | **[35]** |
| Mgo/P(VDF-TrFE) | ... | ... | ... | ... | 2 | ... | ... | 2018 | **[36]** |
| Pi@BCZT and PVDF | ... | 130 | 1.025 | ... | ... | ... | ... | 2017 | **[37]** |
| $BaTiO_3$ and PDMS | ... | ... | ... | 261.40 | 2.67 | 0.1841 | ... | 2016 | **[38]** |

From the literature review it is observed that there are very few reports on the BCZT/PVDF. So this work has well prospective in achieving the better results for BCZT/PVDF due to high value of piezoelectric coefficient of BCZT.

# CHAPTER 3
## Experimental details

### 3.1 Synthesis of BCZT nanoceramics

$Ba_{0.85}Ca_{0.15}Ti_{0.9}Zr_{0.1}O_3$ (BCZT) was synthesised by the sol-gel method which can be also read as the SG-BCZT method. The chemicals used for the preparation of BCZT nanoceramics were analytical reagent grade chemicals with purity greater than 99%, Barium acetate ($Ba(CH_3COO)_2$) , Zirconium oxychloride ($ZrOCl_2 .8H_2O$), calcium nitrate tetra hydrate ($Ca(NO_3)_2.4H_2O$) and titanium isopropoxide ($C_{12}H_{28}O_4Ti$) are the starting materials used for the synthesis of BCZT nanoceramics. Stiochiometric ratio of Zirconium oxychloride ($ZrOCl_2 .8H_2O$) and the calcium nitrate tetra hydrate ($Ca(NO_3)_2.4H_2O$) were dissolved in ethanol separately and are stirred vigorously for 30 minutes until it gets completely dissolved to form a transparent solution. These solutions were mixed together and stirred. Further required stiochiometric compositions of Barium acetate ($Ba(CH_3COO)_2$) was added in the acetic acid and stirred for 30 minutes till it gets completely dissolved. Now, the required amount of the titanium isopropoxide ($C_{12}H_{28}O_4Ti$) is added to the solution and the white solution formed is continuously stirred over night at 80℃, results in a formation of white gel. The gel was further dried at 100 $^0$C the solidified lumps were grounded to the fine powder using the agate mortar and pestle, the synthesis procedure for the preparation of BCZT is shown in Fig 3.1.

The synthesised powder was calcined at different temperatures ranging from 800 $^0$C to 1100 $^0$C for soaking time 6 hours to remove the impurities and the unreacted materials from the synthesised powder. The calcined powder was checked with X-ray diffraction to confirm the phase formation

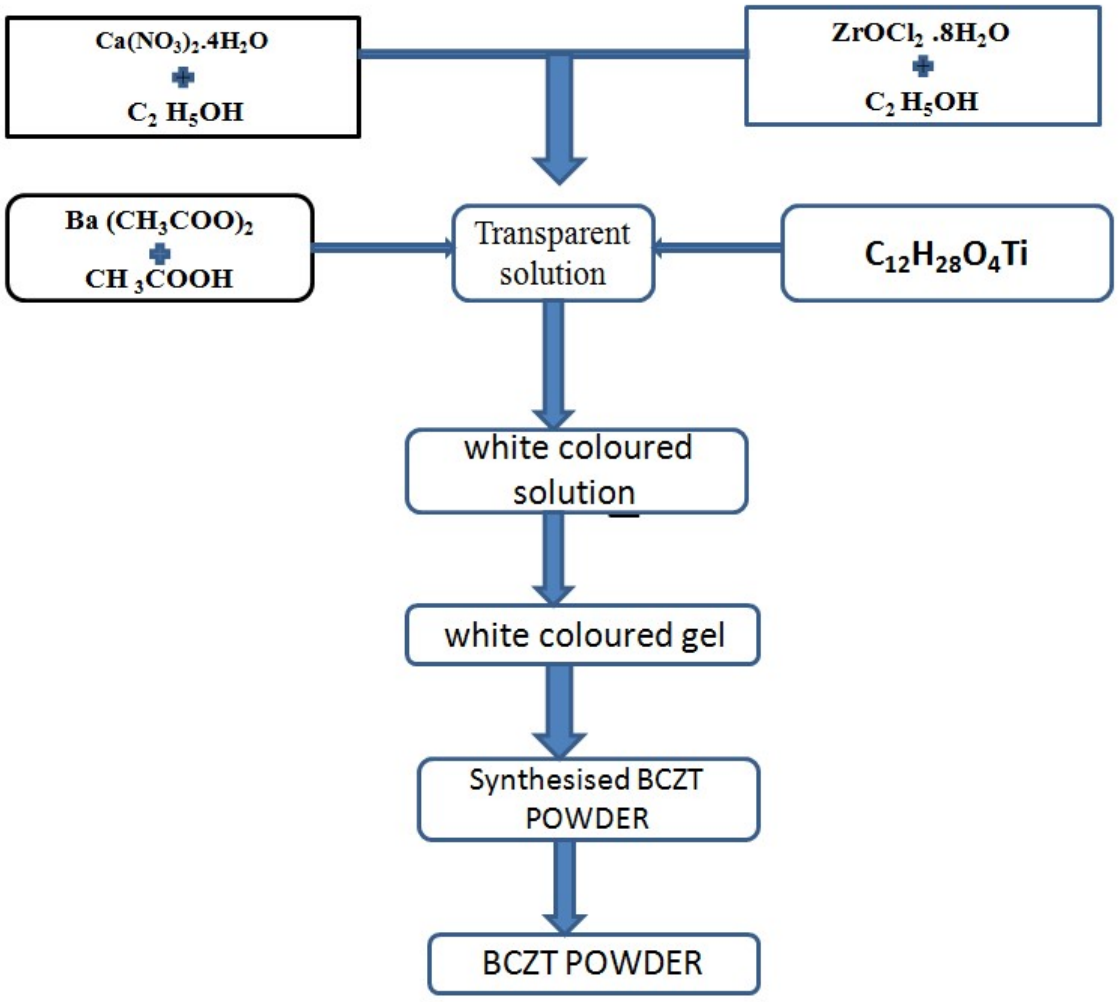


**Fig 3.1 Flow chart of the procedure followed for synthesis of BCZT nanoceramics**

## 3.2 Syntheses of PVDF thin films

### 3.2.1 Materials

Polyvinylidene fluoride (PVDF) is procured from the ALDRICH with average Mw 534,000 for the preparation of PVDF films. N, N-dimethyl formamide (DMF) (LOBA CHEMIE) is used as the solvent.

### 3.2.2 Synthesis of the homogenous solution of PVDF

The PVDF powder was dissolved in the polar solvent Dimethyl formamide (DMF) which is the best solvent for the dissolution of the PVDF. It helps to prepare the thin film with less Porosity and has the higher evaporation rate. The concentration of the PVDF depends upon the desired viscosity, 40% of PVDF by weight is added in 6 ml of DMF to make the homogenous solution. It was placed on the hotplate with continuous stirring for 1hour to completely dissolve the PVDF.

### 3.2.3 Synthesis of the PVDF films by tape casting method

The homogenous solution of PVDF prepared is poured on the glass plate, and then with help of the doctor blade PVDF films of different thickness were fabricated. The films thus formed on the glass plate are dried further at temperature 90℃ . The film is peeled off from the glass plate when it gets completely dried. Thus, by following the above mentioned method flexible, transparent thick films can be fabricated. As shown in the fig 3.2

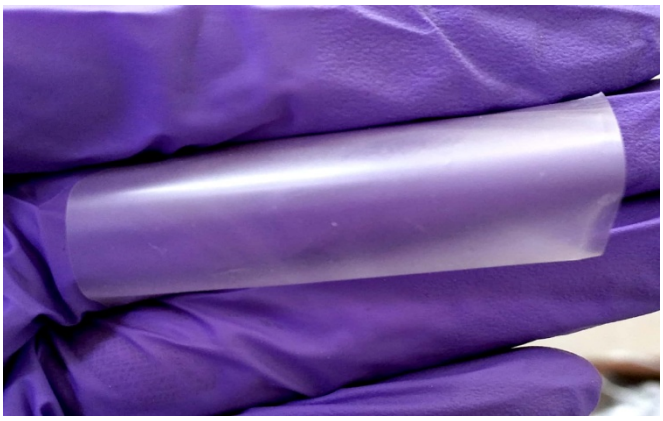

**Fig 3.2 PVDF thin films obtained after drying at 90℃**

## 3.3 Fabrication of BCZT/PVDF composite films

The BCZT/PVDF composite films were prepared by the sol gel process. PVDF powder was brought into the sol form. The PVDF polymer was dissolved into the N, N-dimethylformamide (DMF) at the temperature of 90℃ and the solution was stirred for 1hour on the hot plate till the solution becomes transparent solution. Further the BCZT powder was added in to the DMF and sonicates it for the 1hour. This will helps for complete dissolution of the BCZT powder into the PVDF .This solution was then stirred on hotplate till the solvent gets evaporated and the solution is converted into the gel. The gel was then poured on the glass plate and with the help of the doctor blade BCZT/PVDF composite films were prepared. The concentration of the BCZT was varied in the range of 20%, 30%, 40%, and 50% by weight to get the desired film with no porosity. A BCZT/PVDF composite thin films is shown in fig 3.3

**Fig 3.3 BCZT/PVDF composite film after drying at 80℃ and peeled off from the glass plate**

## 3.4 characteristics

The X-ray diffractometer ("PANalytical X'Pert-Pro MPD PW3040/60 XRD", Cu target X-Ray tube, range $3^0$ to $100^0$ step size 0.02) was used to know the phase composition of the samples. For the presence of the Vibrational modes in all the samples, the FTIR (Fourier transform infrared) spectra of all the samples were obtained by the Fourier Spectrometer (Perkin Elmer Spectrum GX, scan range 15600 to 30 $cm^{-1}$). Thermal analysis was done to know the calcinations temperature and the instrument used is Perkin Elmer TGA (temperature range 1000℃, sensitivity 0.0001mg, atmosphere Air. To know the surface morphology Scanning electron microscope (SEM, JEOL), Dielectric spectrometer was used to know the dielectric constant and the dielectric loss.

### 3.4.1 X-ray Diffractometry (XRD)

X−ray Powder Diffraction (XRD) is a useful procedure for determine the grain size, network constants, solution composition and degree of the crystallinity in crystalline substances. It is mostly used to study the crystalline dimensions, atomic spacing, crystal structure, lattice parameters, phase analysis. This data is useful for the synthesis of material for its structure and its properties.

XRD is based on the constructive interference between the monochromatic x-rays and the crystalline sample. The x-rays are produced by a cathode ray tube, when the electron has the sufficient energy to eject the inner shell electrons of the target material, characteristic X-ray spectra is produced the most common is $K_\alpha$ and $K_\beta$. These x-rays are filtered to produce the monochromatic radiation. Most common target material for single−crystal diffraction is Copper, with CuKα radiation = 0.5418Å. The X-rays are collimated to concentrate and is directed towards the sample. When the

incident rays interact with the sample then they produce the constructive interference, when the conditions are satisfying Bragg's law ($n\lambda = 2d\sin\theta$) as shown in fig 3.4.1(a). These diffracted X-rays are detected, processed and counted. When the sample is scanned through a range of 2θ angles all the diffraction patterns are obtained, d- spacing helps in the identification of mineral [22].

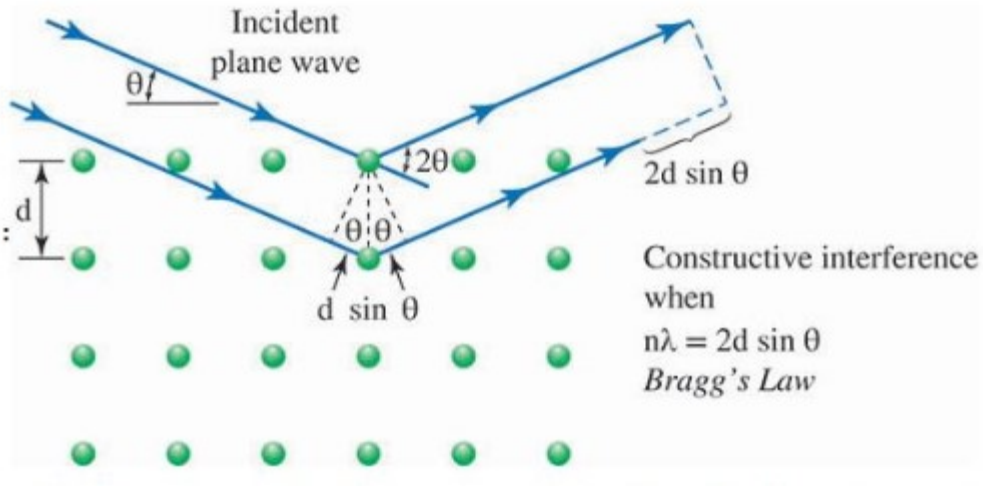


**3.4.1(a) A schematic of Bragg's reflection from a crystal**

Experimental set up for XRD is shown in fig 3.4.1(b)

**Fig 3.4.1(b) Experimental set up of X−ray diffractometer ("PANalytical X'Pert-Pro XRD)** [Ref 22]

**Specification**

| | | |
|---|---|---|
| Model | : | "PANalytical X'Pert-Pro MPD PW3040/60 XRD" |
| Source | : | Cu target X−Ray tube |
| X−Ray Power | : | 2 kW |
| Accuracy | : | ± 0.0025 |
| 2θ° Measurement range | : | 30 to 100 |

### 3.4.2 Fourier transforms infrared (FTIR) spectroscopy

Infrared spectroscopy is a technique which is help to recognize the presence of the functional groups of the molecules and it also detects the presence of specific impurities. It is based on information of internal vibrations of specific frequencies of the molecules; these frequencies are produced in the infrared region in the range of ~ 4000 $cm^{-1}$ to ~ 200 $cm^{-1}$.

When the infrared radiation falls on the sample, the sample absorbs those frequencies which will be corresponding to the molecular Vibrational frequencies and all the other radiations are transmitted by the sample and the frequencies of the absorbed radiations is measured by the infrared spectrometer and the plot of the energy absorbed vs frequency is called infrared spectrum of the material. With the help of this technique it is possible to identify the substance because different material has different vibrations and every material yields different infrared spectra [22].

The basic components of FTIR are shown in fig 3.4.2(a)


**Fig 3.4.2(a) Basic components of FTIR**

1. Source: - Black body source emits the infrared beam, which passes through the aperture which controls the amount of energy that falls on the sample

2. The Interferometer: - The beam passes through the interferometer where the "spectral encoding" occurs. The resulting signal then exits the interferometer.

3. The Detector: - For final measurement beam passes to the detector. The detector measures the special interferogram signal.

4. The Computer: - The signal which is measured by the detector is digitized and sent to the computer for the analysis and the Fourier transformation takes place.

Experimental set up of FTIR spectrometer is shown in the fig 3.4.2(b)

**Fig 3.4.2(b) Experimental set up of FTIR spectrometer**

**Specification**

Model : Perkin Elmer

Scan range : 15600 to 30 $cm^{-1}$

Scan time : 20scan/second

Resolution : 0.15 $cm^{-1}$

Detector : MIRTGS

## 3.4.3 Scanning electron microscope (SEM)

Scanning electron is important instrument which is used to analyze the microstructure of the materials. The main parts of the SEM are electron column, detectors, scanning system, and electronic controls and vacuum system. Electron column consists of the electron gun and the electromagnetic lenses. The electron gun produces the high energy electron beam and electron lenses focuses the electron beam on the specimen. With the help of the scanning coils the beam is focused on the surface of the specimen for scanning. When the accelerated electrons hits the surface of the specimen a signal is emitted in the form of electromagnetic

radiation these are used for the formation of the images and chemically analyse the micro structural constituents. Either the signal may be back scattered electron signal in which there is change in the direction of the motion while as the kinetic energy of the electron remains unchanged or the scattering of the electron may be inelastic scattering where the energy is transferred to the target atoms and electrons which results change in the kinetic energy of the electron beam. The signals are collected by the detector; the resulting signal is amplified and displayed on the monitor [39]. The experimental set up of the SEM is shown in the fig 3.4.3.

**Fig 3.4.3 Experimental set up of scanning electron microscope (SEM)**

**Specifications**

Model : JSM SEM

Magnification : × 5 to × 300,000

Accelerating voltage : 0.5 kV to 30 kV

Resolution : 3.0 nm（30 kV）、8 nm（3 kV）、15 nm（1 kV）

## 3.4.4 Thermogravimetry analysis (TGA)

For thermal analysis of the material the technique which is used is known as Thermogravimetry. It is based on the weight loss of the material as function of temperature or time. In case of isothermal mode the weight changes as a function of time. Thermal analysis plays important role for material characterisation. TGA is based on the mass change of the material. TGA analysis is important to know the thermal events like, absorption, adsorption,

desorption oxidation etc. It also gives information about the loss of the volatile elements during the chemical reaction. It is useful in predicting thermal stability materials. The main factors which effect the mass change are as follows nature of the sample, environment used, heating or cooling rate, and the nature of the sample holder .Specifications (a) temperature range 1500℃ (b) heating rate 0.01 to 100 ℃ (c) sample pans Alumina and platinum (d) Balance sensitivity: 0.1 µg [40]. The instrumental set up of the TGA analyser is shown in fig; 3.4.4

**Fig 3.4.4 Thermogravimetry Analyser**

**Specification**

Model : PERKIN ELMER

Temperature range : Ambient to 1500℃

Heating rate : 0.01 º to 100 º C/min

Atmosphere : Air, Inert gas, 01 º Vacuum

Sample pans : Alumina and platinum

Balance sensitivity : 0.1 µg

# CHAPTER 4

## Results and discussions

### 4.1 X-ray diffraction (XRD) analysis

The X-ray diffraction pattern of the BCZT ceramics calcined at different temperatures is represented in fig 4.1. The pattern is indexed using ICDS NO.-01-089-1428 in the cubic structure with P4mm space group. The peaks correspond to (100), (110), (111), (200) and (211) were attributed to the BCZT with cubic perovskite structure [28]. The Calcination temperatures were varied from 900℃ to the 1100℃ for 6hrs to study the effect of temperature on the phase formation. The optimized calcinations temperature in this study is ~900 $^{0}$c which is much less than that of the solid state reaction process due to the small size of the synthesised powder.

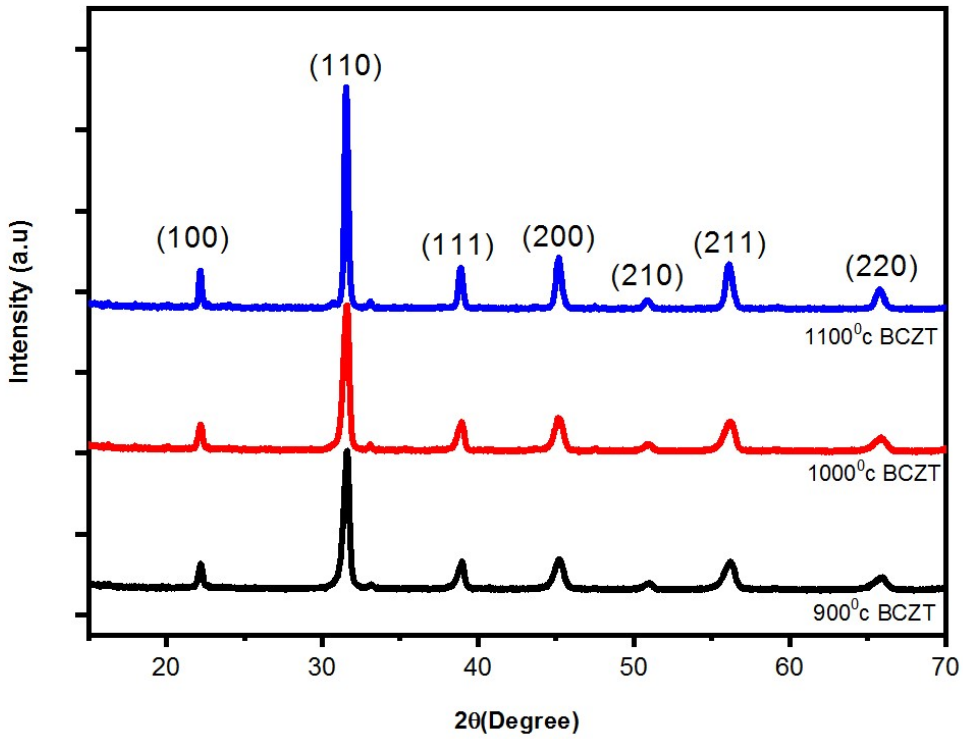


**Fig 4.1 X-ray diffraction pattern of BCZT ceramics calcined at different temperatures.**

The crystallite size (t) of the calcined powder is calculated by following Debye-Scherer relation (Equation 4.1)

$$t = 0.9\lambda / \beta \cos\theta \qquad (4.1)$$

where, 0.9 is shape factor, λ is the wavelength of the x-rays used , β is the broadening of the line at half maximum intensity in degrees (FWHM) and θ is the Bragg's angle. It is observed that the crystallite size increases with an increase in the calcinations temperatures. The average crystallite size for 900 ℃ BCZT calcined powder is ~24nm, while as for 1100 ℃ BCZT calcined powder it is ~ 40nm.

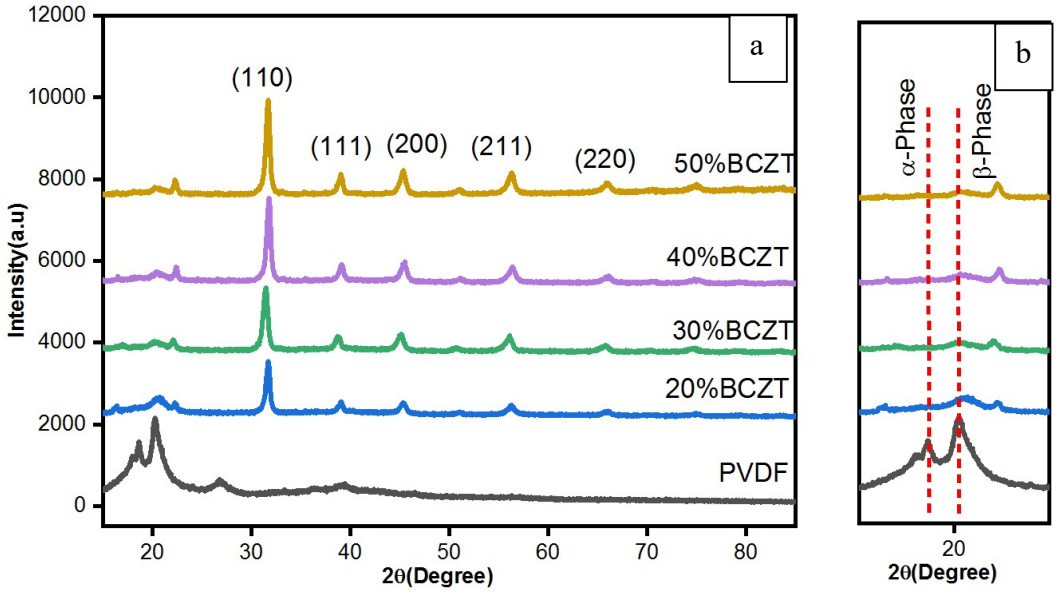


**Fig 4.1(a) and (b) X-ray diffraction pattern of BCZT/PVDF composite films recorded with different wt% of BCZT in the PVDF matrix.**

The X-ray diffraction pattern of the BCZT/PVDF composite thin films with different concentrations of BCZT varying from 20-50% is shown in the fig 4.1(a). The peak at $18.5^0$ is assigned to α-PVDF, while the peak at $20^0$ is assigned to the β-phase; the peak at $26.6^0$ is assigned to the γ-phase. There is no sign of impurity peaks in the XRD pattern. From the figure 4.1(b) it is clear that after the incorporation of the BCZT in the PVDF matrix the peaks corresponding to the PVDF shows the reduction in the intensity while as the diffraction peaks which were assigned to the BCZT becomes clearly visible. The peak intensity of PVDF reduces with an increase in concentration of the BCZT while as the BCZT peaks become sharper and stronger. This is due to increasing the inorganic components the intensity of the crystallized phase peaks became stronger and the crystallinity is much higher [28, 41].

## 4.2 Structural analysis of PVDF thin films

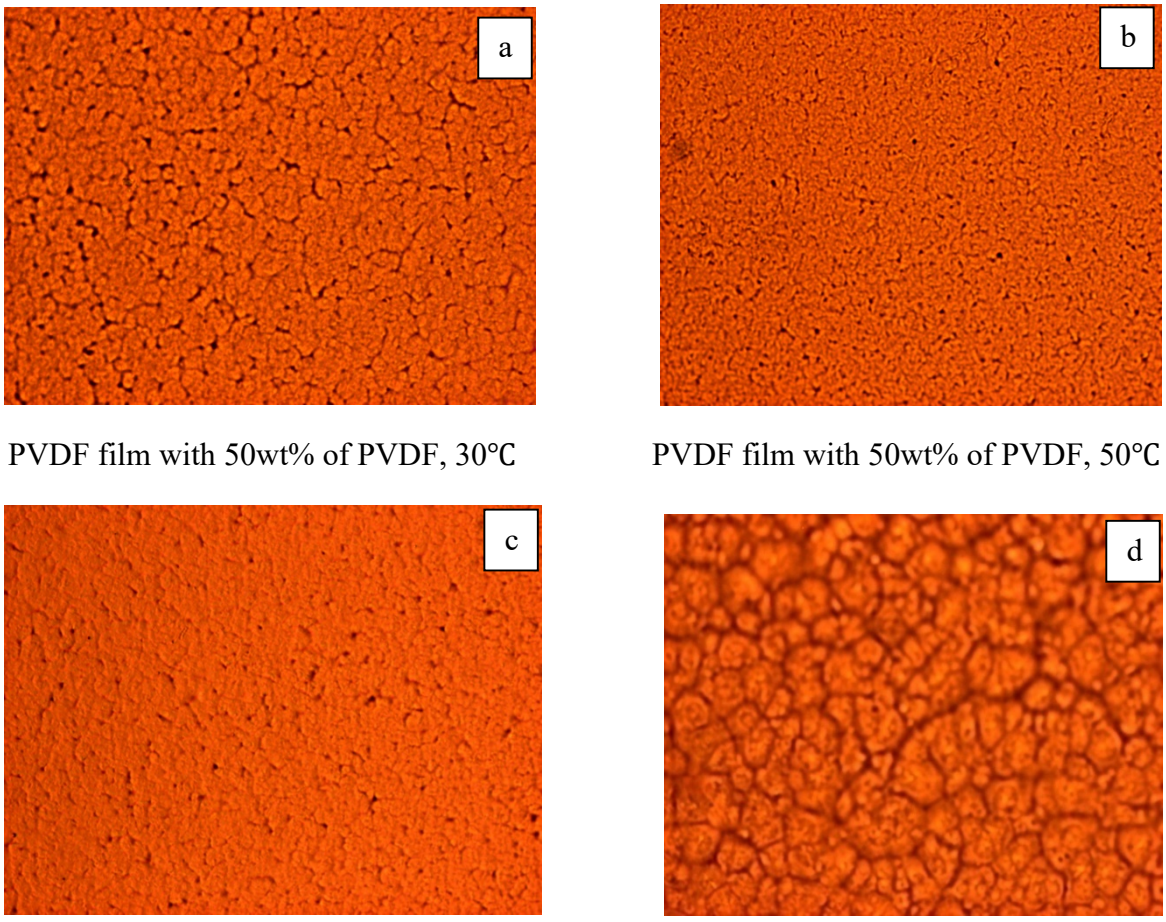


PVDF film with 50wt% of PVDF, 30℃ PVDF film with 50wt% of PVDF, 50℃

PVDF film with 50wt% of PVDF, 70℃ PVDF film with 50wt% of PVDF, 90℃

**Fig 4.2 optical microscopy images of the PVDF thin film with different concentrations of PVDF and different temperature**

Fig 4.2 shows the optical microscopy images of the PVDF thin films at different concentrations and temperatures. It is observed that the PVDF thin film with 20wt% concentration of PVDF and baking temperature 30℃ is more porous, while as PVDF thin film with 50wt% of PVDF and baking temperature 90℃ is less porous and the grain boundaries are also visible. There occurred reduction in the porosity with an increase in baking temperature and concentration of PVDF. As the increasing of PVDF concentration prevents the air bubbles to vent into the solvent during baking thus it helps in reducing the porosity of the films [42]. With increasing the temperature the PVDF spheres coalesce, at 90 ℃ smooth thin films are obtained which are homogeneous, dense and pore free.

## 4.3 SEM morphology of the BCZT/ PVDF composite films

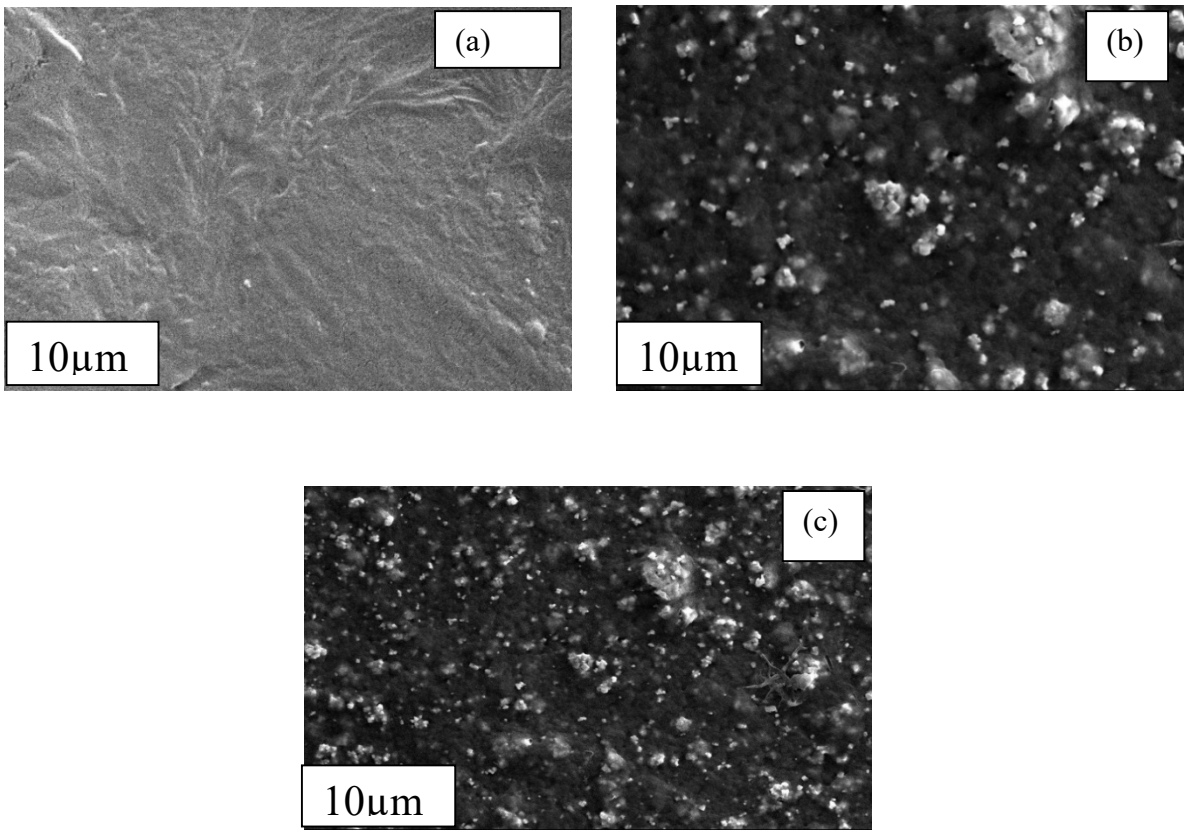


**Fig 4.3 SEM images of PVDF thin film (a) and BCZT/PVDF composite films (b,c) with 40 and 50 wt% of BCZT**

Fig. 4.3 represents the SEM images of the PVDF thin film and BCZT/PVDF composite film. From the SEM image of PVDF thin film fig 4.3 (a) it is clearly visible that the PVDF thin film is neat, clear and free from pores and impurities. Also Fig 4.3(b), 4.3 (c) shows the SEM images of the BCZT/PVDF composite films with 40 and 50 wt% of BCZT nanoceramic particles respectively, it is observed that with increasing the concentration of BCZT nanoceramic particles the packing of the particles grew dense which represents that there is good compatibility between the PVDF matrix and the BCZT nanoceramic particles. In these composite films two regions are observed one is dark region and the other is bright, the dark region is the PVDF matrix and the bright particles are the inorganic BCZT nanoceramic particles. The BCZT nanoceramic particles are homogenously dispersed in the PVDF matrix [28].

## 4.4 Thermal analysis of synthesised BCZT powder

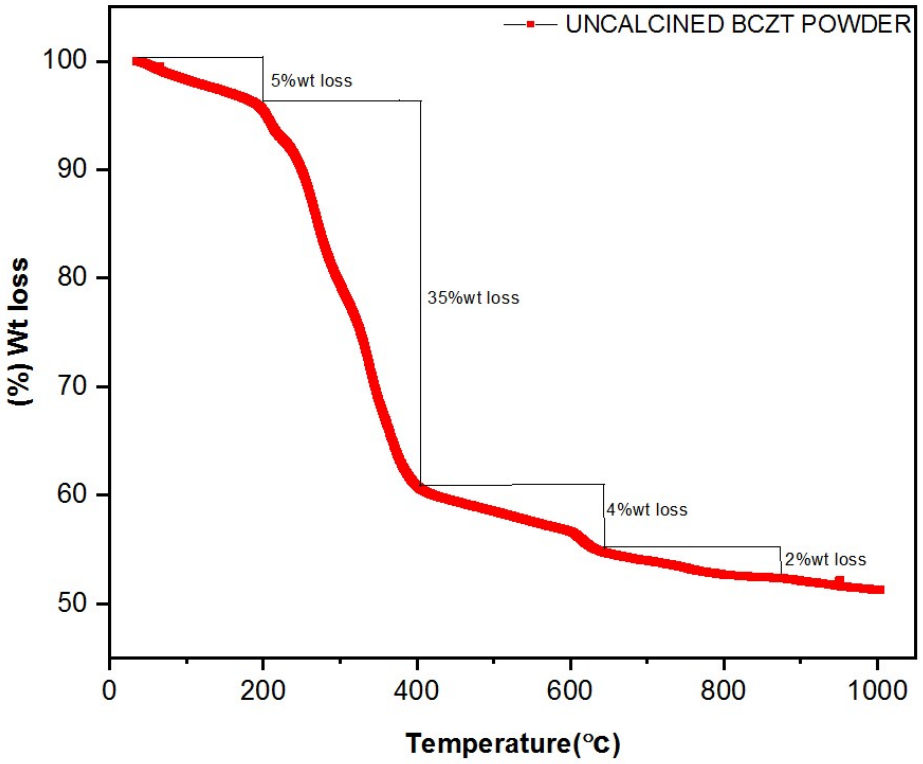


**Fig 4.4 Thermal analysis of the as prepared BCZT powder**

The thermogravimetry (TG) thermograph of uncalcined BCZT is shown in the Fig 4.4. the TGA curve obtained for the uncalcined BCZT powder can be summarized in four stages. The initial stage where the temperature is from 0 to 200℃, the mass loss of uncalicined BCZT powder is attributed to the moisture in the powder and the percentage of the mass loss is 5%. During the the second stage, where the temperature ranges fromm 200 to 405 ℃ ,the precentage of the weight loss is 35%, the weight loss is due to the dissociation of the acetate and alkoxide organic groups, which decomposes into low molecular organics and carbon dioxide. At the third stage where the temperature ranges from 400 to 890℃, the TGA curve shows the 4%wt loss which is attributed to the formation of crystallization of BCZT. In fourth stage there is only 2%wt loss and beyond this at higher temperature the TGA curve is smooth and doesn't show any mass loss which is the indication that calcinations process has finished [43]. Hence gives the calcination temperature of the BCZT powder .

## 4.5 FTIR studies of BCZT/PVDF composite films

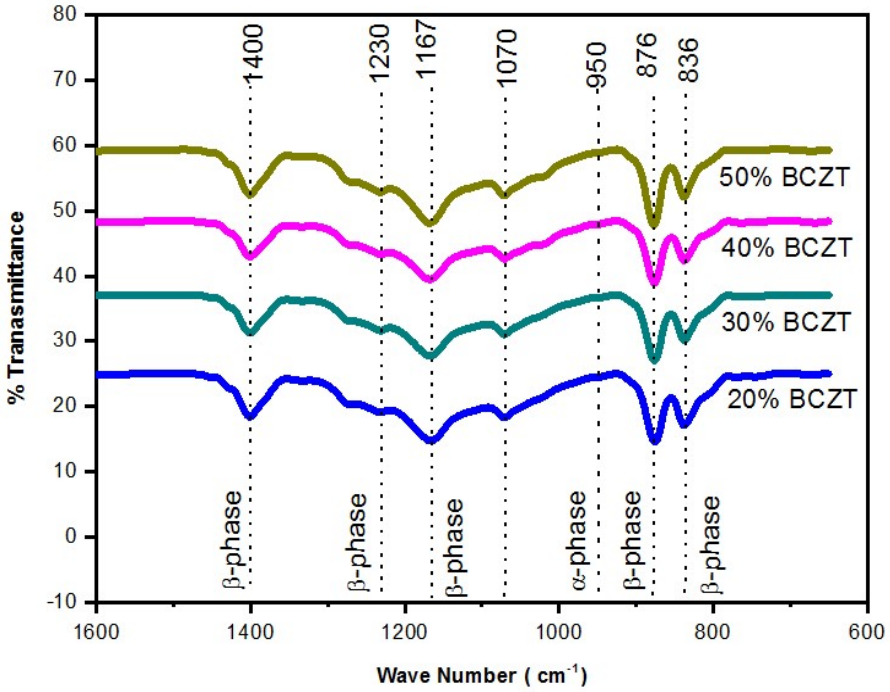


**Fig 4.5 FTIR Spectra of the BCZT/PVDF composite films with different concentration of BCZT nanoceramics, synthesized at 80℃ .**

The FTIR spectra of the BCZT/PVDF composite films are depicted in the figure 4.5 with increasing wt% the BCZT nanoceramics. The signature of the peaks observed at 836, 876, 1167 and 1230 $cm^{-1}$ corresponds to the β-phase of PVDF. The absorbance band at 876 $cm^{-1}$ is assigned to the rocking of the $CH_2$ and the stretching of the $CF_2$ where as the bands observed at 1167 $cm^{-1}$ and 1230 $cm^{-1}$ are attributed to the $CH_2$ wagging and the rocking . The band observed at 1400 $cm^{-1}$ is attributed to the bending of the $CH_2$. The other band 1070 $cm^{-1}$ corresponds to bending of C-C-C. The band at 1019 $cm^{-1}$ starts resolving with the increasing wt% of the BCZT nanoceramics. The polar β-phase which was observed in this affects the crystalline phase of PVDF and this phase is most desirable [28].

## 4.6 Dielectric properties of BCZT/PVDF composite films

The dielectric constant and the Dielectric loss tangent of the BCZT/PVDF composite films as a function of the frequency at room temperature are shown in Fig 4.6. It is observed that the dielectric constant increase with increasing the concentration of the BCZT nanoceramics and

decreases slightly with the increase in frequency. At 50wt% concentration of BCZT nanoceramics, the dielectric constant increased greatly as that of pure PVDF and reaches to 100 at $10^2$ Hz.

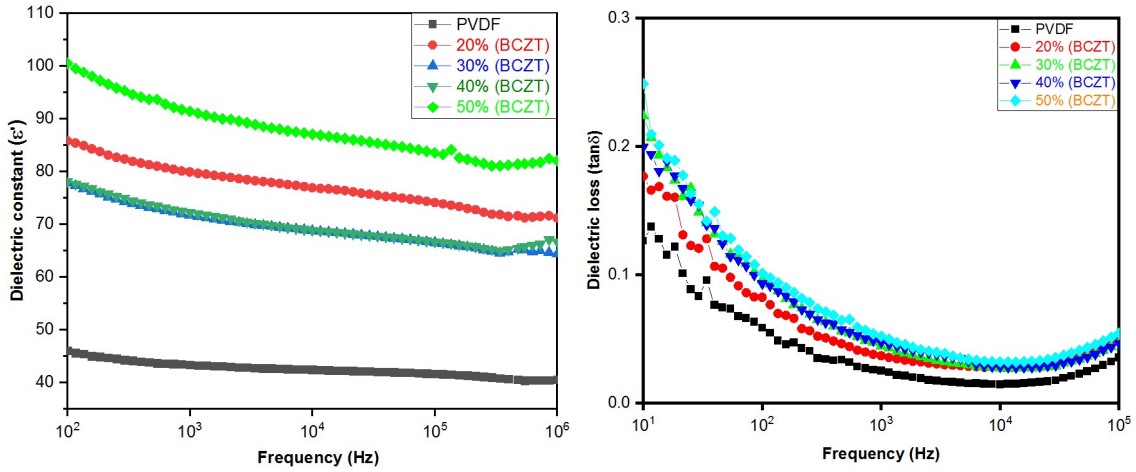


**Fig 4.6 Dielectric constant and dielectric loss of BCZT/PVDF nanocomposite films with different wt% of BCZT.**

The reason behind the increase in dielectric constant with increasing the concentration can be explained as; the high dielectric constant BCZT nanoceramic leads to enhancement of the average electric field in the matrix and by increasing the more content of the BCZT nanoceramic, there will be large dielectric constant contribution. The other reason for the dielectric constant increase is, due to the difference between the BCZT particles and the PVDF matrix, there will be large amount of the charge accumulation on the interfaces of two phases forming interfacial polarisation. So, with increasing the concentration of the BCZT nanoceramics there will be larger amount of the interfacial charges which in turn increases the interfacial polarisation density which raises the dielectric constant. The dielectric loss remains low for all the composites with the slight variation at low frequency. The dielectric loss depends on the distortional, dipolar and the interfacial polarisation. By increasing the BCZT nanoceramic concentration there will be increase in the interfacial area and the PVDF chains gets separated into the smaller domains due to the increased conductivity network. This may lead to the increase in the dielectric loss with the increase in BCZT nanoceramic concentrations. At higher frequency there is rapid increase in the dielectric loss which leads to relaxation of the peak at high frequency. This is attributed to α relaxation process which is due to the glass transition of PVDF [1, 28]. The highest dielectric constant is 91.35 and tanδ is 0.05 at 1K Hz.

# CHAPTER 5

## Conclusion and future scope

## 5.1 Conclusions

BCZT ceramic powder was synthesised by the sol-gel method. Composite films of BCZT/PVDF were prepared through solution casting method. After calcining the synthesised powder at different temperatures, single phase perovskite structure was obtained at 900℃. The calcinations temperature of the synthesised BCZT powder was also confirmed by the thermal analysis (TGA) i.e. 900℃. SEM results confirmed that the particles of BCZT are homogeneously in the PVDF matrix. Optical pictures also confirmed that with increasing concentration of PVDF porosity decreases. XRD and the FTIR results confirmed the formation of the β-phase in the composite films. The dielectric constant increases with increase in the concentration of BCZT particle and dielectric loss do not show much variation in frequency range of $10^3$ to $10^5$Hz. The highest dielectric constant is 91.35 and tanδ is 0.05 at 1K Hz.

## 5.2 Future scope

- Piezoelectricity can serve as the great source of "GREEN ENERGY".
- Flexible piezoelectric materials are interesting for energy application due to their ability to withstand the large stress.
- Convert the environmental vibratory energy into the electric energy
- The power supply can be used to power other devices or can be stored for later use.
- It will be interesting to see the effects of BCZT on the power characteristics of the device.

# REFRENCES


1 Aniket Patra, Avijit Pal, Shrabanee Sen, Polyvinylpyrrolidone modified barium zirconate titanate /polyvinylidene fluoride nanocomposite as self-powered sensor, Ceramics International 44 (2018) 11196–11203

2 Z.L. Wang, J. Song, Piezoelectric nanogenerators based on zinc oxide nanowire Arrays, Science 312 (2006) 242–246.

3 Z. Wen, M.H. Yeh, H. Guo, J. Wang, Y. Zi, W. Xu, J. Deng, L. Zhu, X. Wang, C.Hu, L.Zhu, X. Sun, Z.L. Wang, Self-powered textile for wearable electronics by hybridizing fiber-shaped nanogenerators, solar cells and supercapacitors, Sci. Adv. 2 (2016) 1600097–1600104.

4. Z.L. Wang, Self powered Nanosensors and Nanosystems, Adv. Mater. 24 (2012) 280 – 285.

5. Y. Wu, Z.L. Wang, Recent progress in piezoelectric nanogenerators as a sustainable Power source in self powered systems and active sensors, Nanoenergy 14 (2015) 3–14.

6 M. Yuan, L. Cheng, Q. Xu, W. Wu, S. Bai, Z.L. Wang, Biocompatible nanogenerator With 209 V output voltage directly powers a light emitting diode, Nano Lett. 13 (2013) 91–94.

7. B. Kumar, S.W. Kim, Energy harvesting based on semiconducting piezoelectric ZnO Nanostructures, Nano Energy 1 (2012) 342–355.

8. S. Paria, S.K. Karan, R. Bera, A.K. Das, A. Maitra, B.B. Khatua, A facile approach to Develop a highly stretchable PVC/ZnSnO3 piezoelectric nanogenerator with high output power generation for powering portable electronic devices, I&EC Res. 55 (2016), 10671–10680.

9 E. Fukada, T. Furukawa, Piezoelectricity and ferroelectricity in polyvinylidene Fluoride, Ultrasonics 19 (1981) 31–39.

10 Saito Y, Takao H, Tani T, Nonoyama T, Takatori K, Homma T, et al. Lead-freepiezoceramics. *Nature* 2004; 432:84–7.

11 X. Wang , H.L.W. Chan, C.L. Choy, J. Am. Ceram. Soc. 86 (2003) 1809-1811.

12 B. Jaffe, W.R. Cook, H.L. Jaffe, Piezoelectric Ceramics, Academic Press, London, 1971.

13 T. Takenaka, H. Nagata, J. Eur. Ceram. Soc. 25 (2005) 2693-2700.

14. P.K. Panda, J. Mater. Sci. 44 (2009) 5049-5062.

15 Liu W, Ren X. Large piezoelectric effect in Pb-free ceramics. *Phys Rev Lett*2009; **103**(257602):1–4.

16 Gao J, Xue D, Wang Y, Wang D, Zhang L, Wu H, et al. Microstructure basis for strong piezoelectricity in Pb-free Ba(Zr0.2Ti0.8)O3–(Ba0.7Ca0.3)TiO3ceramics. *Appl Phys Lett* 2011; **99**(092901):1–3.15

17 A. Salimi, A.A. Yousefi, FTIR studies of β-phase crystal formation in stretched PVDF films, Polym. Test. 22 (2003) 699–704.

18 Jain A, Prashanth KJ, Sharma AK, Jain A, Rashmi PN. Dielectric and piezoelectric Properties of PVDF/PZT composites: a review. *Polym Eng Sci*. 2015; 55(7):1589 - 1616.

19 Kim HS, Kim JH, Kim J. A review of piezoelectric energy harvesting based on vibration. *Int J Precis Eng Manuf*. 2011;12(6):1129 - 1141.

20 Boris Gusarov, PVDF piezoelectric polymers: characterization and application to thermal energy harvesting, 2015

21 Young Zhang, Huajun sun, Wen Chen, A brief review of Ba ($Ti_{0.8}$ $Zr_{0.2}$)$O_3$-($Ba_{0.7}Ca_{0.3}$)$TiO_3$ based lead free piezoelectric ceramics; Past, present and future perspectives , J. Of physics and chemistry of solids (2018) 207-219

22 Nikita H. Patel, Basic Principle, Working and Instrumentation of Experimental Techniques, July−2015

23 J. Paul Praveen, T. Karthik, A.R. James, E. Chandrakala, Saket Asthana, Dibakar Das, Effect of poling process on piezoelectric properties of sol–gel derived BZT–BCT ceramics, Journal of the European Ceramic Society 35 (2015) 1785–1798.

24 Zhongming Wang, Juanjuan Wang, Xiaolian Chao,Lingling Wei, Bian Yang, Dawei Wang Zupei Yang, Synthesis, structure, dielectric, piezoelectric, and energy storage performance of ($Ba_{0.85}Ca_{0.15}$)($Ti_{0.9}Zr_{0.1}$)$O_3$ ceramics prepared by different methods, Journal of Materials Science Materials in Electronics, (2016) 27:5047–5058.

25 Klara Castkova, Chemical Synthesis, Sintering and Piezoelectric Properties of $Ba_{0.85}Ca_{0.15}Zr_{0.1}Ti_{0.9}O_3$ Lead-Free Ceramics, The American Ceramic Society (2015), 98 [8] 2373–2380.

26 Yang Bai , Ales Matousek , Pavel Tofel , Vijay Bijalwan , Bo Nan, Hana Hughes , Tim W.Button, (Ba,Ca)(Zr,Ti)$O_3$ lead-free piezoelectricceramics—The critical role of

processing onproperties, Journal of the European Ceramic Society 35 (2015) 3445–3456

27 Bhoopesh mahale , Dhananjay bodas and S a gangal, Study of β-phase development in spin-coated PVDF thick films**,** Bull. Mater. Sci., Vol. 40, No. 3, June 2017, pp. 569–575.

28 Yueping wang and Zhijian PENG, Performance of $Ba_{0.95}Ca_{0.05}Zr_{0.15}Ti_{0.85}O_3$/PVDF Composite flexibe films, Journal of the ceramics society of japan (2014)122[8] 719-724 .

29 Sai Pavan Prashanth Sadhu, Sasidhar Siddabattuni, Sai Muthukumar V, K. B. R. Varma, Enhanced dielectric properties and energy storage density of surface engineered BCZT/PVDF-HFP nanodielectrics, Journal of Materials Science: Materials in Electronics (2018) 29:6174–6182.

30 S. Crossley, R. A. Whiter and S. Kar-Narayan, Polymer-based nanopiezoelectric generators for energy harvesting applications, Materials Science and Technology 2014 VOL 30 NO. 13a, 1613.

31 Yanfei Kou, Ziming Kou, Dongping Zhao, Zhijian Wang, Guijun Gao, Xuejun Chai, Fabrication of lead-free $Ba(Zr_{0.2}Ti_{0.8})O_3$–$(Ba_{0.7}Ca_{0.3})TiO_3$ nanoparticles and the application in flexible piezoelectric nanogenerator, *Ceramics International,* Volume 43, 15 April 2017, Pages 4803-4806

32 Bingcheng Luo, Xiaohui Wang, Yueping Wang and Longtu Li, Fabrication, characterization, properties and theoretical analysis of ceramic/PVDF composite flexible films with high dielectric constant and low dielectric loss, J. Mater. Chem. A, 2014, 2, 510–519

33 Manoj Kumar Gupta,Sang-Woo Kim, and Binay Kumar, Flexible High-Performance Lead-Free $Na_{0.47}K_{0.47}Li_{0.06}NbO_3$ Microcube-Structure-Based Piezoelectric Energy Harvester, ACS Appl. Mater. Interfaces (2016), 8, 1766−1773.

34 Huidrom Hemojit Singh | Simrjit Singh | Neeraj Khare, Enhanced β-phase in PVDF polymer nanocomposite and its application for nanogenerator, Polym Adv Technol. 2018; 29:143–150

35 Prakriti Adhikary and Dipankar Mandal, Enhanced electro-active phase in a luminescent P(VDF–HFP)/$Zn^{2+}$ flexible composite film for piezoelectric based energy harvesting applications and self-powered UV light detection, *Phys. Chem. Chem. Phys.,* 2017, 19, 17789—17798

36 Deepa Singh, Aditya Choudhary, and Ashish Garg, Flexible and Robust Piezoelectric Polymer Nanocomposites Based Energy Harvesters, ACS Appl. Mater. Interfaces 2018, 10, 2793−2800'

37 Haowei Lu, Jiaqi Lin, Wenlong Yang, Lizhu Liu, Improved dielectric strength and loss tangent by interface modification in PI@BCZT/PVDF nano-composite films with high permittivity, Mater Electron (2017) 28:13360–13370.

38 Jing Yan and Young Gyu Jeong, High Performance Flexible Piezoelectric Nanogenerators based on $BaTiO_3$ Nanofibers in Different Alignment Modes, ACS Appl. Mater. Interfaces 2016, 8, 15700−15709

39 R.K. Sindhu, scanning electron microscope.

40 T. C. Daniels Thermal Analysis, John Wiley & Sons, Hanser Publisher, NewYork (1973).

41 S. Lanceros-Méndez, J. F. Mano, A. M. Costa and V. H. Schmidt, J. Macromo. Sci., Part B, 40, 517527 (2001).

42 Yuh-Chung Hu, Wei- li- Hsu,Yi-Ta-Wang, Cheng-Tao Ho and Pei-Zen Chang, Enhance of pyroelectricity of Polyvinylidene Flouride by Graphene-oxide Doping, sensors(2014),14,6877-6890

43 Xiang Ji, Chuanbin Wang, Songbin Li, Song Zhang, Rong Tu, Qiang Shen, Ji Shi, Lianmeng Zhang, Structural and electrical properties of BCZT ceramics synthesized by sol–gel process, Materials in Electronics (2018) 29:7592–7599